

# GPDs of the nucleons and elastic scattering at high energies

O.V. Selyugin\*

*BLTP, Joint Institute for Nuclear Research,*

## Abstract

Taking into account the electromagnetic and gravitational form factors, calculated from a new set of  $t$ -dependent GPDs, a new model is built. The real part of the hadronic amplitude is determined only through complex  $s$ . In the framework of this model the quantitative description of all existing experimental data at  $52.8 \leq \sqrt{s} \leq 1960$  GeV, including the Coulomb range and large momentum transfers ( $0.0008 \leq |t| \leq 9.75$  GeV<sup>2</sup>), is obtained with only 3 fitting high energy parameters. The comparison with the preliminary data of the TOTEM Collaboration at an energy of 7 TeV is made.

## 1 Introduction

The dynamics of strong interactions finds its most complete representation in elastic scattering at small angles. Only in this region of interactions we can measure the basic properties of the non-perturbative strong interaction which define the hadron structure: the total cross section, the slope of the diffraction peak and the parameter  $\rho(s, t)$ . Their values are connected, on the one hand, with the large-scale structure of hadrons and, on the other hand, with the first principles which lead to the theorems on the behavior of the scattering amplitudes at asymptotic energies [1, 2].

There are indeed many different models for the description of hadron elastic scattering at small angles [3, 4]. They lead to the different predictions for the structure of the scattering amplitude at asymptotic energies, where the diffraction processes can display complicated features [5]. This concerns especially the asymptotic unitarity bound connected with the Black Disk Limit (BDL) [6]. In Chow-Yang model [7, 8] it was assumed that the hadron interaction to be proportional the overlapping of the matter distribution of the hadrons and in Wu and Yang [7] suggested that the matter distribution is proportional to the charge distribution of the hadron. Then many model were used the electromagnetic form factors of hadron, but, in most part they change his form to describe the experimental data, as was made in the famous Bourrely-Soffer-Wu model [9]. The parameters of the obtained form-factor are determined by the fit of the differential cross sections.

Now we present a model that used two form factors determined by one function - generalized parton distributions (GPDs). Following sum rules valid for the momentum of the

---

\*selugin@theor.jinr.ru

GPDs [10, 11] the integration over the momentum fraction,  $x$ , yields the conventional electromagnetic form factors and the integration of the next momentum of the GPDs [10, 12] yields the gravitation form factors. The correlation between hadron form factors and energy momentum tensor were discussed long time ago [13] and recently [14, 15]. So, both the form factors are independent of the fitting procedure of the differential cross sections. Note that the form of the GPDs is determined, on the one hand, by the deep-inelastic processes and, on the other hand, by the measure of the electromagnetic form factor from the electron-nucleon elastic scattering. Hence, the form of the electromagnetic form factor (first momentum of GPDs) determines the form of the second form factor (second momentum of GPDs). This scheme is supported by the good description of the experimental data in the Coulomb-hadron interference region and large momentum transfer at high energies of one amplitude with a few free parameters.

The impact of the hard pomeron contribution on the elastic differential cross sections is very important for understanding the properties of the QCD in the non-perturbative regime [16]. Note, that the real part of the hard pomeron is essentially large then the real part of the soft pomeron. Now in [17] it is suggested that such a contribution can be explained by the preliminary result of the TOTEM Collaboration [18] on the elastic proton-proton differential cross sections. In our model, the real part of the hadronic amplitude is determined only through complex  $s$  satisfying the cross symmetric relation. In the framework of this model, the quantitative description of all existing experimental data at  $52.8 \leq \sqrt{s} \leq 1960$  GeV, including the Coulomb range and large momentum transfers  $0.0008 \leq |t| \leq 9.75$  GeV<sup>2</sup>, is obtained with only 3 fitting high energy parameters. The comparison of the predictions of the model at 7 TeV and preliminary data of the TOTEM collaboration are shown to coincide well. There is some small place, especially in the region of the diffraction dip, for the small correction contributions which are determined by the odderon, and possibly the spin-dependent part of the scattering amplitude which gives a small contribution at large momentum transfer. In the framework of the model, only the Born term of the scattering amplitude is introduced. Then the whole scattering amplitude is obtained as a result of the unitarization procedure of the hadron Born term that is then summed with the Coulomb term. The Coulomb-hadron interference phase is also taken into account. The essential moment of the model is that both parts of the Born term of the scattering amplitude have the positive sign, and the diffraction structure is determined by the unitarization procedure.

The electromagnetic and hadronic parts of the elastic scattering amplitudes used in the model are presented in the second and third sections. In the fourth section, we introduce the hadron form factors obtained from the first and second momenta of GPDs. Our fitting procedure and the description of the high energy differential cross sections of the proton-proton and proton-antiproton scattering are presented in the fifth and sixth sections. Also, we stretch our model on 7 TeV and compare the model calculations with the preliminary data of the TOTEM Collaboration. Then, the model calculations are compared with the experimental data at low energies  $\sqrt{s} = 30$  GeV. In the seventh section and in the conclusion, we show and discuss the model calculations for the total cross sections and the value of  $\rho(s, t)$  obtained in the framework of the model.

## 2 Electromagnetic part of the hadron scattering amplitude

The differential cross sections of nucleon-nucleon elastic scattering can be written as the sum of different helicity amplitudes:

$$\frac{d\sigma}{dt} = \frac{2\pi}{s^2} (|\Phi_1|^2 + |\Phi_2|^2 + |\Phi_3|^2 + |\Phi_4|^2 + 4|\Phi_5|^2). \quad (1)$$

The total helicity amplitudes can be written as  $\Phi_i(s, t) = F_i^h(s, t) + F_i^{em}(s, t)e^{i\varphi(s, t)}$ , where  $F_i^h(s, t)$  comes from the strong interactions,  $F_i^{em}(s, t)$  from the electromagnetic interactions and  $\varphi(s, t)$  is the interference phase factor between the electromagnetic and strong interactions [19, 20, 21]. For the hadron part the amplitude with spin-flip is neglected in this approximation, as usual at high energy.

The electromagnetic amplitude can be calculated in the framework of QED. In the high energy approximation, it can be obtained [22] for the spin-non-flip amplitudes:

$$F_1^{em}(t) = \alpha f_1^2(t) \frac{s - 2m^2}{t}; \quad F_3^{em}(t) = F_1^{em}; \quad (2)$$

and for spin-flip amplitudes:

$$F_2^{em}(t) = \alpha \frac{f_2^2(t)}{4m^2} s; \quad F_4^{em}(t) = -F_2^{em}(t), \quad (3)$$

$$F_5^{em}(t) = \alpha \frac{s}{2m\sqrt{|t|}} f_1(t) f_2(t),$$

where the form factors are:

$$f_1(t) = \frac{4m_p^2 - (1+k)t}{4m_p^2 - t} G_d(t); \quad (4)$$

$$f_2(t) = \frac{4m_p^2 k}{4m_p^2 - t} G_d(t);$$

with  $k$  relative to the anomalous magnetic moment, and  $G_d(t)$  has the conventional dipole form

$$G_d(t) = 1/(1 - t/0.71)^2. \quad (5)$$

## 3 Main hadronic amplitude

The model is based on the representation that at high energies a hadron interaction in the non-perturbative regime is determined by the reggeized-gluon exchange. The cross-even part of this amplitude can have two non-perturbative parts, possible standard pomeron ( $P_{2np}$ ) and cross-even part of the three non-perturbative gluons ( $P_{3np}$ ) case. The interaction of these two objects is proportional to two different form factors of the hadron. This is the main assumption of the model. Of course, we cannot insist on the origin of the second term of the scattering amplitude. It can be of a different nature. However, in any case, it has the

high energy parameters			low energy parameters	
$h_1, \text{ GeV}^{-2}$	$h_2, \text{ GeV}^{-2}$	$\epsilon_1$	$r_1, \text{ GeV}$	$r_2, \text{ GeV}$
$1.03 \pm 0.02$	$3.31 \pm 0.02$	$0.11 \pm 0.01$	$11.95 \pm 0.5$	$-5.9 \pm 0.8$

Table 1: The basic parameters of the model are determined by fitting experimental data.

cross-even properties and positive sign. The second important assumption is that we chose the slope of the second term 4 time smaller than a slope of the first term, by analogy with the two pomeron cut. Both terms have the same intercept.

The form factors are determined by the General parton distributions of the hadron (GPDs). The first form factor, corresponding to the first momentum of GPDs is the conventional electromagnetic form factor -  $G(t)$ . The second form factor is determined by the second momentum of GPDs -  $A(t)$ . The parameters and  $t$ -dependence of the GPDs are determined by the standard parton distribution functions, so by the experimental data on the deep-inelastic scattering, and by the experimental data for the electromagnetic form factors (see [23]).

Hence, the Born term of the elastic hadron amplitude can be written as

$$F_h^{Born}(s, t) = h_1 G^2(t) F_a(s, t) (1 + r_1/\hat{s}^{0.5}) + h_2 A^2(t) F_b(s, t) (1 + r_2/\hat{s}^{0.5}) \quad (6)$$

where  $F_a(s, t)$  and  $F_b(s, t)$  has the standard Regge form

$$F_a(s, t) = \hat{s}^{\epsilon_1} e^{B(s) t}; \quad F_b(s, t) = \hat{s}^{\epsilon_1} e^{B(s)/4 t}, \quad (7)$$

with  $G(t) = G_E(t)$  is the Sachs electric form factor relative to the first moment of GPDs and  $A(t)$  relative to the second moment of GPDs.

$$G(t) = \frac{L_1^4}{(L_1^2 - t)^2} \frac{4m_p^2 - (1+k)t}{4m_p^2 - t} \quad (8)$$

$$A(t) = \frac{L_2^4}{(L_2^2 - t)^2}. \quad (9)$$

with the parameters:  $L_1^2 = 0.71 \text{ GeV}^2$ ;  $L_2^2 = 2 \text{ GeV}^2$ .

$$\hat{s} = s e^{-i\pi/2}/s_0; \quad s_0 = 1 \text{ GeV}^2. \quad (10)$$

The slope of the scattering amplitude has the standard logarithmic dependence on the energy.

$$B(s) = \alpha' \ln(\hat{s}). \quad (11)$$

with  $\alpha' = 0.24 \text{ GeV}^{-2}$ .

The final elastic hadron scattering amplitude is obtained after unitarization of the Born term. So first, we have to calculate the eikonal phase

$$\chi(s, b) = \frac{1}{2\pi} \int d^2q e^{i\vec{b}\cdot\vec{q}} F_h^{Born}(s, q^2), \quad (12)$$

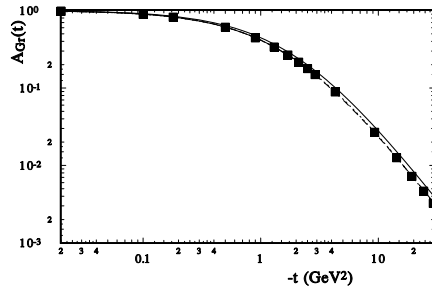


Figure 1: The hadron form factor  $A(t)$  - (the second momentum of GPDs) in the  $t$  representation ( squares - the numerical calculation of the integral over  $x$  is normalized to 1, hard line - the dipole form with  $L^2 = 2.0 \text{ GeV}^2$ ). dashed line - the dipole form  $L^2 = 1.8 \text{ GeV}^2$ ).

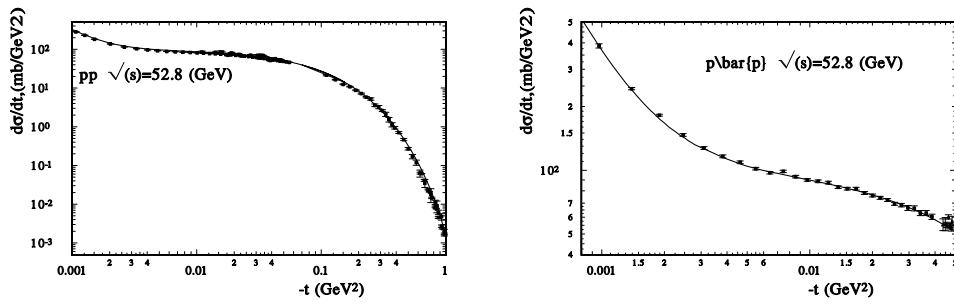


Figure 2:  $d\sigma/dt$  at  $\sqrt{s} = 52.8 \text{ GeV}$  and at small  $t$  for  $pp$  (left) and for  $p\bar{p}$  (right).

and then obtain the final hadron scattering amplitude

$$F_h(s, t) = is \int b J_0(bq) \Gamma(s, b) db. \quad (13)$$

$$\Gamma(s, b) = 1 - \exp[-\chi(s, b)]. \quad (14)$$

All these calculations are carried out by the FORTRAN program.

## 4 Hadron form factors

As was mentioned above, all the form factors are obtained from the GPDs of the nucleon [23]. The electromagnetic form factors can be represented as first moments of GPDs

$$F_1(t) = \int_0^1 dx \sum_{u,d} \mathcal{H}^q(x, t); \quad F_2(t) = \int_0^1 dx \sum_{u,d} \mathcal{E}^q(x, t), \quad (15)$$

following from the sum rules [10, 11].

Let us modify the original Gaussian ansatz in order to incorporate the observations of [24] and [25] and choose the  $t$ -dependence of GPDs in the form

$$\mathcal{H}^q(x, t) = q(x) \exp[a_+ \frac{(1-x)^2}{x^m} t]. \quad (16)$$

The value of the parameter  $m = 0.4$  is fixed by the low  $t$  experimental data while the free parameters  $a_{\pm}$  ( $a_+$  - for  $\mathcal{H}$  and  $a_-$  - for  $\mathcal{E}$ ) were chosen to reproduce the experimental data in the whole  $t$  region. Indeed, large  $t$  behavior corresponds to  $x \sim 1$  in (10), (11), where the dependence on  $m$  is weak.

The function  $q(x)$  was chosen at the same scale  $\mu^2 = 1$  as in [26], which is based on the MRST2002 global fit [27]. In all our calculations we restrict ourselves, as in other quoted work, to the contributions of  $u$  and  $d$  quarks.

Hence, we have

$$u(x) = 0.262x^{-0.69}(1-x)^{3.50}(1 + 3.83x^{0.5} + 37.65x), \quad (17)$$

$$d(x) = 0.061x^{-0.65}(1-x)^{4.03}(1 + 49.05x^{0.5} + 8.65x). \quad (18)$$

With this simple form we obtained a good description of the proton electromagnetic Sachs form factors. Using the isotopic invariance we obtained good descriptions of the neutron Sachs form factors without changing any parameters [23].

We shall use this model of GPDs to obtain the second momentum form factor of the nucleon. Taking instead of the electromagnetic current  $J^\mu$  the energy-momentum tensor  $T_{\mu\nu}$  together with a model of quark GPDs, one can obtain the gravitational form factor of fermions [23, 12] For  $\xi = 0$  one has

$$\int_0^1 dx x \sum_{u,d} [\mathcal{H}(x, t) \pm \mathcal{E}(x, t)] = A_h(t) \pm B_h(t). \quad (19)$$

The integration of the second momentum of GPDs over  $x$  gave the momentum-transfer representation of the form factor (see Fig. 1). We approximate this by the dipole form

$$A(t) = L_2^4 / (L_2^2 - t)^2. \quad (20)$$

with the parameter  $L_2^2 = 2.0 \text{ GeV}^2$ .

## 5 Fitting procedure

The model has only three high energy fitting parameters and two low energy parameters, which reflect some small contribution coming from the different low energy terms. (see Table 1). We take all existing experimental data in the energy range  $52.8 \leq \sqrt{s} \leq 1960$  GeV and the region of the momentum transfer  $0.0008 \leq -t \leq 9.75$  GeV<sup>2</sup> of the elastic differential cross sections of proton-proton and proton-antiproton data [28, 29]. So we include the whole Coulomb-hadron interference region where the experimental errors are remarkably small. We do not include the data on total cross sections  $\sigma_{tot}(s)$  and  $\rho(s)$ , as their values were obtained from the differential cross sections especially in the Coulomb-hadron interference region. Including such data decreases  $\chi^2$ . We also do not include the interpolated and extrapolated data of Amaldi [30].

In the fitting procedure we calculate the minimum in  $\sum_{i=1}^N \chi_i^2$  related with the statistical errors  $\sigma_i^2$ . The systematical errors are taken into account by the additional normalization coefficient  $n_k$  for the  $k$  series (the experiment) of the experimental data

$$\chi^2 = \sum_{i=1}^N \frac{n_k E_i(s, t) - T_i(s, t)}{\sigma_i^2(s, t)}. \quad (21)$$

where  $T_i(s, t)$  are the theory predictions and  $n_k E_i(s, t)$  are the data points allowed to shift by the systematical error of the  $k$ -experiment (see, for example [31, 32]).

In the region of the small momentum transfer the systematic errors are of an order of  $2\% \div 5\%$ . For most part the additional normalization are in the region  $0.95 \div 1.05$ . At large momentum transfer the order of the systematical errors is  $10\% \div 20\%$ . In this case, the additional normalization is situated in the region  $0.8 \div 1.2$ .

For the non-normalized experimental data of the UA4/2 Collaboration [33], which have very small statistical errors, we take the normalization determined in [34]. Our correction normalization is obtained from the fitting procedure in this case  $n_{UA42} = 0.95$ .

As a result, one obtains  $\sum \chi_i^2/N \simeq 1.8$  where  $N = 975$  is the number of experimental points. Of course, if one sums the systematic and statistical errors, the  $\sum \chi^2/N$  decreases, to 1.4. Note that the parameters of the model are energy-independent. The energy dependence of the scattering amplitude is determined only by the single intercept and the logarithmic dependence on  $s$  of the slope.

Note that there are some separate points ( $n = 17$ ) at the different energies and momentum transfer which give  $\sum_{n=1}^{17} \chi_n^2 = 260$ . However, we do not remove such points.

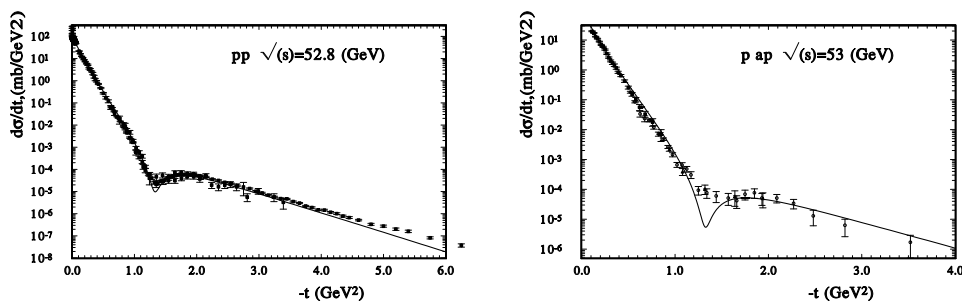


Figure 3:  $d\sigma/dt$  at  $\sqrt{s} = 52.8$  GeV at large  $|t|$  for  $pp$  (top) and for  $\bar{p}p$  (bottom panel)

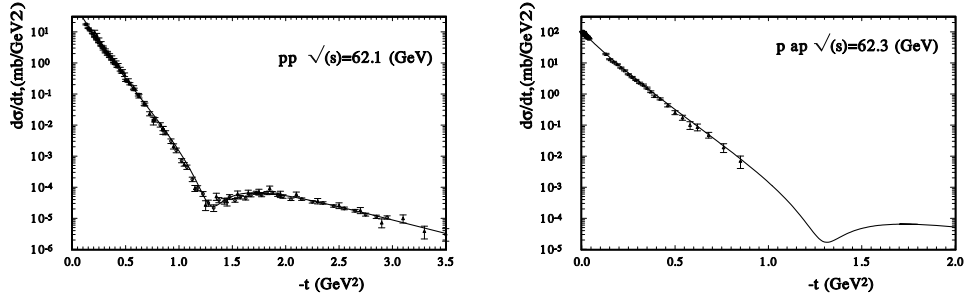


Figure 4:  $d\sigma/dt$  at  $\sqrt{s} = 62.1$  GeV at large  $|t|$  for  $pp$  (left) and for  $\bar{p}p$  (right panel)

## 6 Description of the differential cross sections

The differential cross sections for proton-proton elastic scattering at  $\sqrt{s} = 52.8$  GeV are presented in Fig. 2(left panel) and 3(top panel). At this energy there are experimental data

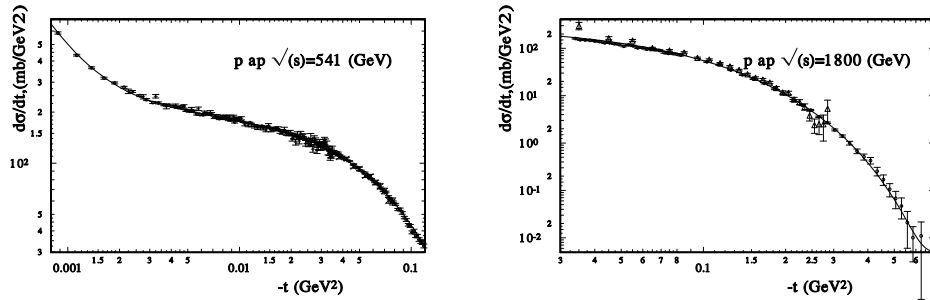


Figure 5:  $d\sigma/dt$  for  $\bar{p}p$  elastic scattering at small momentum transfer, at  $\sqrt{s} = 541$  GeV (top) and  $\sqrt{s} = 1800$  GeV (bottom)

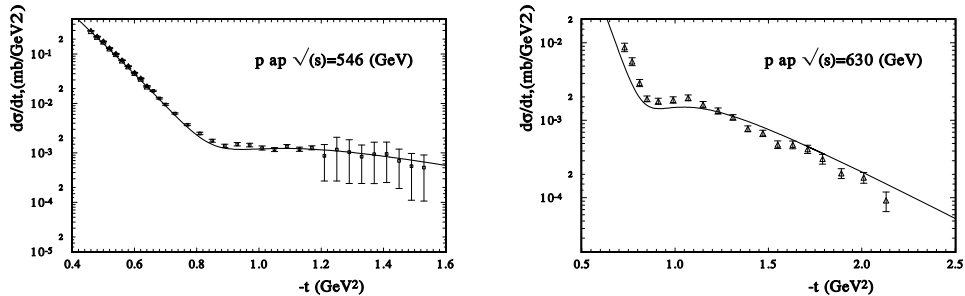


Figure 6:  $d\sigma/dt$  for  $\bar{p}p$  elastic scattering at large  $t$ , at  $\sqrt{s} = 546$  GeV (top) and  $\sqrt{s} = 630$  GeV (bottom panel)

at small (beginning at  $-t = 0.001 \text{ GeV}^2$ ) and large (up to  $-t = 10 \text{ GeV}^2$ ) momentum transfers. The model reproduces both regions and provides a qualitative description of the dip region at  $-t \approx 1.4 \text{ GeV}^2$ , for  $\sqrt{s} = 53 \text{ GeV}^2$  and for  $\sqrt{s} = 62.1 \text{ GeV}^2$  (Fig.3(top) and Fig.4(left panels)).

Now let us examine the proton-antiproton differential cross sections (see Fig. 2(right panel)). In this case at small momentum transfer the Coulomb-hadron interference term plays an important role and has the opposite sign. The model describes the experimental data well. Slightly worse than  $pp$  is the description of  $p\bar{p}$  of differential cross sections at  $\sqrt{s} = 53 \text{ GeV}$ , especially in the diffraction minimum (Fig. 3(bottom panel)).

Maybe, this shows an additional odderon contribution. Note that at  $\sqrt{s} = 62.2 \text{ GeV}$  for  $p\bar{p}$  scattering the description of the differential cross sections is essentially better (Fig. 4).

In Fig. 5, the description of the proton-antiproton scattering at  $\sqrt{s} = 541 \text{ GeV}$  and at  $\sqrt{s} = 1800 \text{ GeV}$  is shown. In these cases, the Coulomb-hadron interference term is large, especially at  $\sqrt{s} = 541 \text{ GeV}$  as  $t$  is very small. The good description of the experimental data shows that the energy dependence of the real part of scattering amplitude obtained in the model corresponds to the real physical situation.

Figures 6 and 7 show the description of the experimental data at larger momentum transfers for  $\sqrt{s} = 546 \text{ GeV}^2$  and  $\sqrt{s} = 630 \text{ GeV}^2$  and for Tevatron energies  $\sqrt{s} = 1800 \text{ GeV}$  and  $\sqrt{s} = 1960 \text{ GeV}$ . It is clear that the model leads to a good description of these data in the region of the diffraction minimum without taking into account the odderon contribution. Hence, it is shown that very likely the intercept of the odderon is near 1.

On basis of this fit of the experimental data at  $52.8 \leq \sqrt{s} \leq 1960 \text{ GeV}$  and  $0.0008 \leq |t| \leq 9.75 \text{ GeV}^2$  we obtained the fitting parameters (see Table 1). Taking into account these values of the parameters we extend the scope of the model and calculate the differential cross sections at 7 TeV for  $pp$  elastic scattering. In Fig. 8, the comparison of the model calculations with the parameters, based at the fit of the existing experimental data at  $52.8 \leq \sqrt{s} \leq 1960 \text{ GeV}$ , with the preliminary data of the TOTEM Collaboration are shown. Except the size of the diffraction minimum the coincidences are remarkable. Of course, if we include in the model some different correction terms, like odderon, the value of the fitting parameters of the model will be slightly change. However, we think that the basic properties of the model will not change in future.

Now let us see how we can extend the scope of the model to a low energy . The calculation

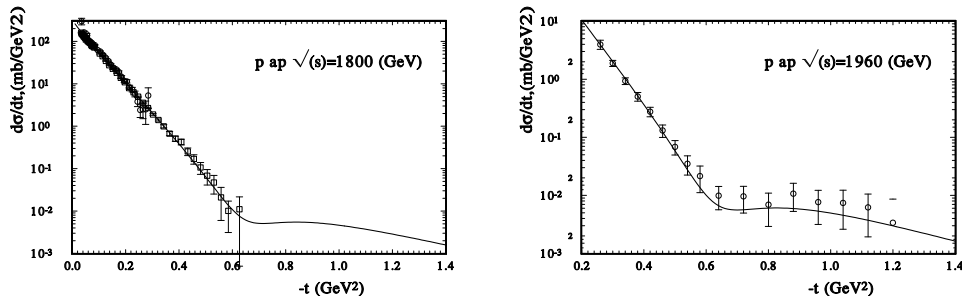


Figure 7:  $d\sigma/dt$  for  $\bar{p}p$  elastic scattering at large  $t$ , at  $\sqrt{s} = 1800 \text{ GeV}$  (top) and  $\sqrt{s} = 1960 \text{ GeV}$  (bottom panel)

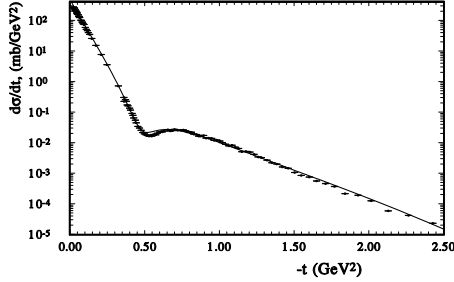


Figure 8: The comparison of the model calculations with the parameters, based on the fit of the experimental data at  $52.8 \leq \sqrt{s} \leq 1960$  GeV, with the preliminary data of the TOTEM Collaboration at  $\sqrt{s} = 7$  TeV.

of the model of  $d\sigma/dt$  for  $\bar{p}p$  and  $pp$  elastic scattering at  $\sqrt{s} = 30.6$  GeV are compared with the experimental data on Fig.9 and Fig.10. There is a very good description at small momentum transfer for both the reactions -  $pp$  and  $\bar{p}p$ . At large  $t$  the model reproduces the differential cross sections only qualitatively. The position of the diffraction minimum corresponds to the experimental data. However, the form of the diffraction minimum obviously requires some additional small correction terms, possibly by the odderon contributions. This situation repeated the problem of describing the form of the diffraction minimum at  $\sqrt{s} = 53$  GeV for  $\bar{p}p$  elastic scattering.

## 7 Energy dependence of $\rho(s, t)$ and $\sigma_{tot}(s)$

The ratio of the real part to the imaginary part of the elastic scattering hadronic amplitude

$$\rho(s, t) = ReF_h(s, t)/ImF_h(s, t)$$

is very important as it reflects the  $t$ -dependence of the both parts of the scattering amplitude, which are connected one to the other through the integral dispersion relations. The validity

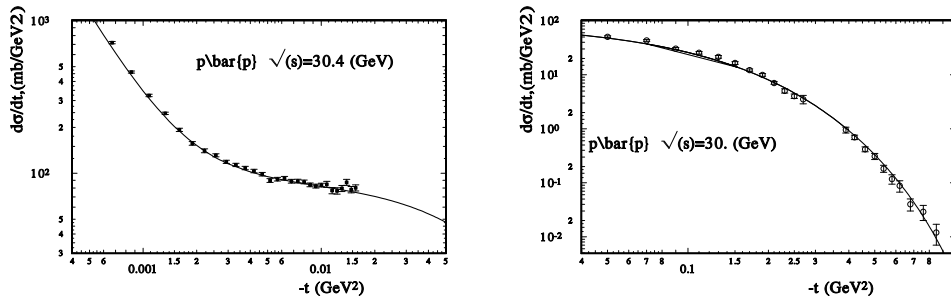


Figure 9: The model predictions of  $d\sigma/dt$  for  $\bar{p}p$  elastic scattering at at  $\sqrt{s} = 30.6$  GeV.

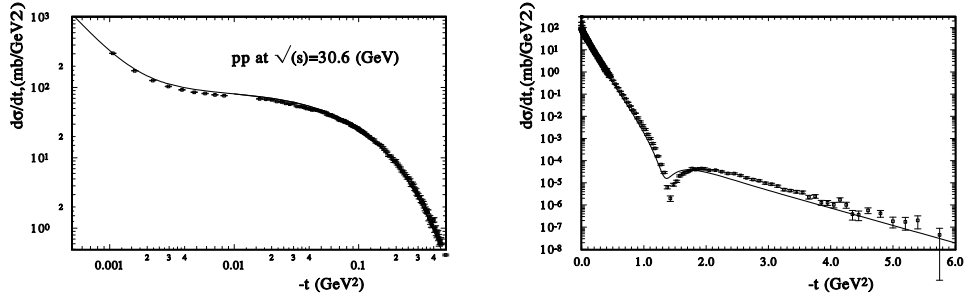


Figure 10: The model predictions of  $d\sigma/dt$  for  $pp$  elastic scattering at at  $\sqrt{s} = 30.6$  GeV.

of this relation can be checked at LHC energies. The deviation can point out the existence of a fundamental length at TeV energies [35, 36]. Usually, the value of  $\rho(s, t = 0)$  is assumed to be small and to vary little with  $t$ :  $\rho(s, t) \approx 0.14$ . The differential cross sections at small momentum transfer  $|t| \leq 0.05$  GeV<sup>2</sup>, the so-called Coulomb-hadron interference region, are determined by the interference of the Coulomb amplitude with the real part of the hadron amplitude. Hence, the  $s$  and  $t$  dependence of the real part of the hadron amplitude, which is reflected in  $\rho(s, t)$ , will determine the form of the differential cross sections.

In the model, the real part of  $F_h(s, t)$  is determined only by the complex cross-symmetric form of energy  $\hat{s} = s \exp[-i\pi/2]$ . No other artificial function or some parameters impact the form or  $s$  and  $t$  dependence of the real part. Despite such simplicity, the model sufficiently well describes the experimental data in the Coulomb-hadron region of momentum transfer and in a wide energy region (see Figs. 2,5,9). The calculated  $\rho(s, t = 0)$  in the model is shown in Fig. 11(top panel). For the most part it coincides with  $\rho$  obtained by the COMPETE Collaboration [37, 38]. We can see that the  $\rho(s, t)$  reaches its maximum 0.135 at approximately 1 TeV and then slowly decreased up to 0.127 at  $\sqrt{s} = 20$  TeV. Note that the model takes into account the only cross-symmetric part of the scattering amplitude.

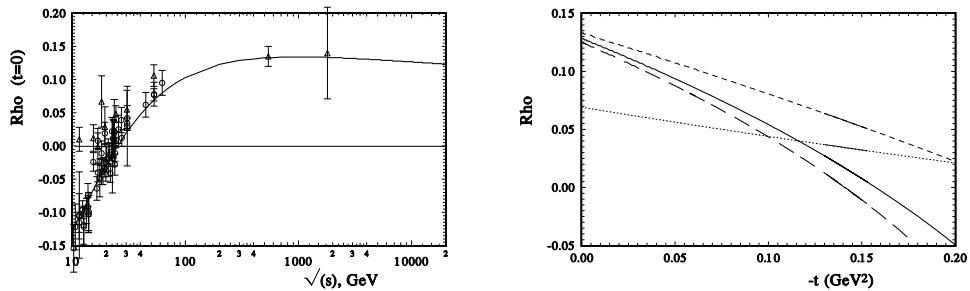


Figure 11:  $\rho(s, t)$  for  $pp$  elastic scattering at  $t = 0$  (top); (circle and triangles are the experimental data of  $pp$  and  $\bar{p}p$  elastic scattering, respectively. and at small momentum transfer (bottom) at  $\sqrt{s} = 52.8$  GeV (tiny-dash line),  $\sqrt{s} = 541$  GeV (dash line),  $\sqrt{s} = 7$  TeV (hard line), and  $\sqrt{s} = 14$  TeV (long-dash line)

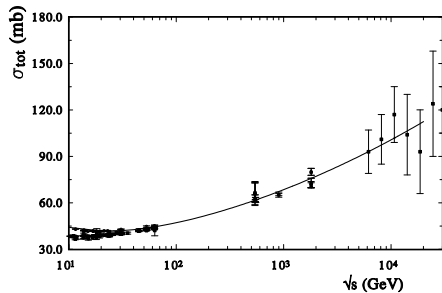


Figure 12:  $\sigma_{tot}(s)$  are calculated in the model (hard line). (circle and triangles are the experimental data of  $pp$  and  $\bar{p}p$  elastic scattering, respectively).

This reflects that at low energy it, in most part, coincides with the experimental data of the proton-proton scattering. The  $t$  dependence of  $\rho$ , shown in Fig. 11(bottom panel), is interesting. We can see that after  $\sqrt{s} = 1$  TeV, where  $\rho$  reaches its maximum, its  $t$ -dependence is changed. If the maximum of  $\rho$  is small decreasing, his slope will be larger and larger. It is interesting to compare this figure with a figure like this in our phenomenological analysis of  $\rho$  at high energies [39]. The size of  $\rho$  is essentially larger, but the dynamic change of  $\rho$  with  $s$  and  $t$  is practically the same. It is related with the saturation regime which impacts on the  $s$  and  $t$  dependence of  $\rho(s, t)$  at high energies.

As the data on the total cross section  $\sigma_{tot}(s)$  and  $\rho(s, t)$  were not included in our fitting procedure, let us now calculate these values in the framework of the model. The energy dependence of the  $\sigma_{tot}(s)$  is shown in Fig. 12. Our model calculations coincide with the existing experimental values sufficiently well. The model calculations gives  $\sigma_{tot} = 43.46, 61.7, 75.76$  mb for the energies -  $\sqrt{s} = 50, 540, 1800$  GeV.

## 8 Conclusion

We present the new model of the hadron-hadron interaction at high energies. The model is very simple from the viewpoint of the number of parameters and functions. There are no any artificial functions or some cuts which bound the separate parts of the amplitude by some region of momentum transfer. The model describes all high energy data sufficiently well, except the form of the diffraction minimum of the proton-antiproton scattering at  $\sqrt{s} = 53$  GeV. As we know, it is the only model which describes all available high energy data in the Coulomb-hadron region and large momentum transfer. The energy dependence of the differential cross sections is determined by only one intercept  $\Delta = 1 + \epsilon$  with  $\epsilon = 0.11$  and the  $\alpha' = 0.24 \ln[\hat{s}]$ . One of the most remarkable properties is that the real part of the hadron scattering amplitude is determined only by complex energy  $s$  that satisfies the crossing-symmetries. The differential cross sections at small momentum transfer are determined, in most part, by the Coulomb-hadron interference term. This is essentially caused by the  $s$  and  $t$  dependence of the real part of the hadronic amplitude. A good description of the differential cross section (see figs 2, 5, 9) confirms the determination of the real part in the model.

However, the most important advantage of the model is that it is built on some physical

basis - two form factors which are calculated from GPDs. The behavior of the differential cross section at small  $t$  is determined, in most part, by the electromagnetic form factors; and at large  $t$ , by the matter distribution (calculated in the model from the second momentum of the GPDs), as was supposed by H. Miettinen a long time ago [40] and then used in the work of S. Sanielevici and P. Valin [41]. Of course, we understand that this advantage of the model, on the other hand, has some disadvantage. Now we have no rigorous proof of such a physical picture. However, the best work of the model maintains the hope that such a representation has a right to exist.

The model predicts  $\sigma_{tot} = 95$  mb at  $\sqrt{s} = 7$  TeV. The preliminary data of the TOTEM show  $\sigma_{tot} = 98.3 \pm 0.2^{stat.} \pm 2.8^{syst.}$  mb [4]. Of course, some correction terms (corresponding to the odderon or spin-flip amplitudes) have to be included in our model. Now the model does not show a contribution of the hard pomeron in the examined energy region. The presence of the hard pomeron has to give an additional contribution in the real part of the scattering amplitude and change the size and form of the Coulomb-hadron interference term [39]. Hence, we hope that all these additional terms will be determined after fitting with the new data of the proton-proton scattering at LHC energies.

**Acknowledgements:** The author would like to thank J.-R. Cudell for helpful discussions, gratefully acknowledges the financial support from BELSPO and would like to thank the University of Liège where part of this work was done.

## References

- [1] A.Martin, F. Cheung, Analytic properties and bounds of the scattering amplitude (New York, 1970).
- [2] S.M.Roy, Phys.Rep. **C 5** (1972) 125.
- [3] R. Fiore, et all., Mod.Phys., **A24** (2009) 2551.
- [4] G. Antchev et all. (TOTEM Coll.), arXiv: 1110.1395.
- [5] J. R. Cudell and O. V. Selyugin, Czech. J. Phys. **54** (2004) A441 [arXiv:hep-ph/0309194].
- [6] O. V. Selyugin, J. R. Cudell and E. Predazzi, Eur. Phys. J. ST **162** (2008) 37 [arXiv:0712.0621 [hep-ph]].
- [7] T.T. Wu and C.N. Yang Phys.Rev., **175** 1832 (1968)
- [8] T.T. Chou and C.N. Yang Phys.Rev., **137** 708 (1965).
- [9] C. Bourrely, J. Soffer, T.T. Wu, Eur.Phys.J. **C28** (2003) 97.
- [10] X.D. Ji, Phys. Lett. **78** , (1997) 610; Phys. Rev D **55** (1997) 7114.
- [11] Radyushkin, A.V., Phys. Rev. D **56**, (1997) 5524.
- [12] O.V. Selyugin, O.V. Teryaev, Foundations of Physics , ISSN:0015-9018 , eISSN:1572-9516).
- [13] H. Pagels Phys.Rev. 144 (1966) 1250).
- [14] M. Polyakov, Phys.Lett. B555 (2003) 57.
- [15] Z. Abidin and C.E. Carlson, Phys.Rev. **D77** (2008) 095007.
- [16] J. R. Cudell, E. Martynov, O. V. Selyugin and A. Lengyel, Phys. Lett. B **587** (2004) 78.
- [17] A. Donnachie, P.V. Landshoff, arXiv:1112.2485
- [18] G. Latino et all. (TOTEM Coll.), arXiv: 1110.1008.
- [19] O.V. Selyugin, Mod. Phys. Lett. **A9** (1994) 1207.
- [20] O.V. Selyugin, Mod. Phys. Lett. **A14**, 223 (1999).

- [21] O. V. Selyugin, Phys. Rev. D **60** (1999) 074028
- [22] N. H. Buttimore, E. Gotsman, E. Leader, Phys. Rev. D **35**, (1987) 407.
- [23] O. Selyugin, O. Teryaev, Phys. Rev. D (2009).
- [24] A. V. Radyushkin, Phys. Rev. D **58** 114008 (1998).
- [25] Burkardt M., Phys.Lett. B **595**, 245 (2004) .
- [26] M. Guidal, M.V. Polyakov, A.V. Radyushkin, and M. Vanderhaeghen, Phys. Rev. D **72** , 054013 (2005)
- [27] A.D. Martin *et al.*, Phys. Lett. B **531** (2002) 216.
- [28] J.-R. Cudell et al.: <http://www.theo.phys.ulg.ac.be/~Cudell/data>.
- [29] Spires Durham data base  
(<http://durpdg.dur.ac.uk/hepdata>).
- [30] U.Amaldi, K.R. Schubert, Nucl.Phys. **B166** 301 (1980).
- [31] A.D. Martin, et al. , Eur.Phys.J. **C70** 189 (2009).
- [32] G. Wattt, arXiv:1201.1295.
- [33] UA42 Coll., C. Augier *et al.*, *Phys. Lett. B* **316**, (1993) 448.
- [34] O. Selyugin, Phys. Lett. **B333**, 245 (1994)
- [35] N.N. Khuri, Proceedings "Results and perspectives in Particle Physics", (M. Grecco ed.), p.701 Gif-nur-Yvette, France (1994).
- [36] C. Bourrely, N.N. Khuri, A. Martin, J. Soffer, T.T. Wu, Proceedings EDS 2005, Blois, France (2005).
- [37] J. R. Cudell *et al.* [COMPETE Collaboration], Phys. Rev. D **65** (2002) 074024; Phys. Rev. Lett. **89** (2002) 201801;
- [38] J. R. Cudell, V. Ezhela, K. Kang, S. Lugovsky and N. Tkachenko, Phys. Rev. D **61** (2000) 034019 [Erratum-ibid. D **63** (2001) 059901].
- [39] J. R. Cudell and O. V. Selyugin, Phys. Rev. Lett. **102** (2009) 032003 [arXiv:0812.1892 [hep-ph]].
- [40] H. Miettinen, Nucl.Phys. B **166** (1980) 365.
- [41] S. Sanielevici, P.Valin, Phys.Rev. D29 (1984) 52.